

Weak Gravitational Lensing

Part II/II

Martin Kilbinger

CEA Paris-Saclay, Irfu/DAP - AIM, CosmoStat; IAP

Euclid Summer School, Banyuls
August 2019

`martin.kilbinger@cea.fr`

`www.cosmostat.org/kilbinger`

Slides: `http://www.cosmostat.org/events/ecole19`



`@energie_sombre`

`#EuclidBanyuls2019`



COSMOSTAT



université
PARIS-SACLAY



Overview

Reminders from last year (part I)

Part II day 1.

- E-/B-modes

- Galaxy-galaxy lensing

- Shear calibration

Reminder from last year ...

Books, Reviews and Lecture Notes

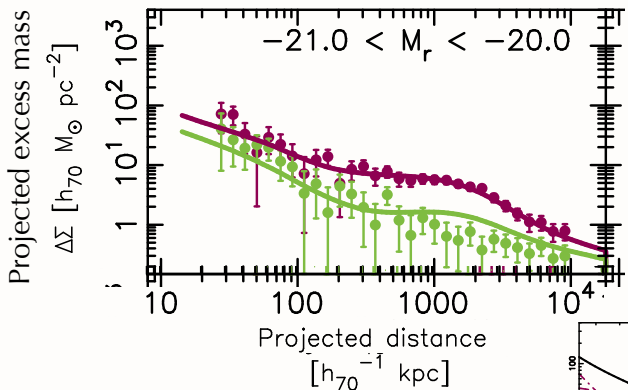
- Bartelmann & Schneider 2001, review **Weak gravitational lensing**, Phys. Rep., 340, 297 arXiv:9912508
- Kochanek, Schneider & Wambsganss 2004, book (Saas Fee) **Gravitational lensing: Strong, weak & micro**. Download Part I (Introduction) and Part III (Weak lensing) from my homepage <http://www.cosmostat.org/people/kilbinger>.
- Kilbinger 2015, review **Cosmology from cosmic shear observations** Reports on Progress in Physics, 78, 086901, arXiv:1411.0155
- Bartelmann & Maturi 2017, review **Weak gravitational lensing**, Scholarpedia 12(1):32440, arXiv:1612.06535
- Mandelbaum 2018, review **Weak lensing for precision cosmology**, ARAA submitted, arXiv:1710.03235
- Henk Hoekstra 2013, lecture notes (Varenna) arXiv:1312.5981
- Sarah Bridle 2014, lecture videos (Saas Fee) <http://archiveweb.epfl.ch/saasfee2014.epfl.ch/page-110036-en.html>
- Alan Heavens, 2015, lecture notes (Rio de Janeiro) www.on.br/cce/2015/br/arq/Heavens_Lecture_4.pdf

Science with gravitational lensing

Outstanding results

Dark matter profiles in outskirts of galaxies.

Measuring halo mass to very large galactic scales.



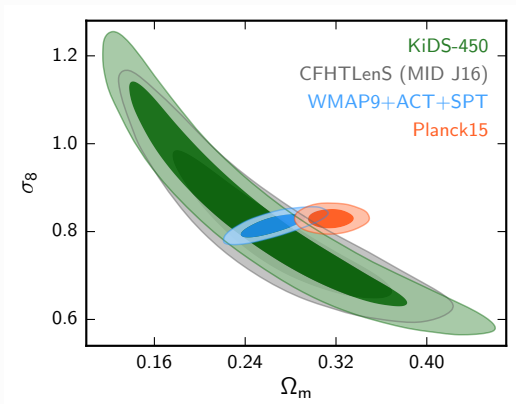
Science with gravitational lensing

Outstanding results

Hints of inconsistency of our cosmological model at low and high z ?

Planck and WL in tension? Also WL cluster masses for Planck SZ clusters;

H_0 from cepheids + SL.

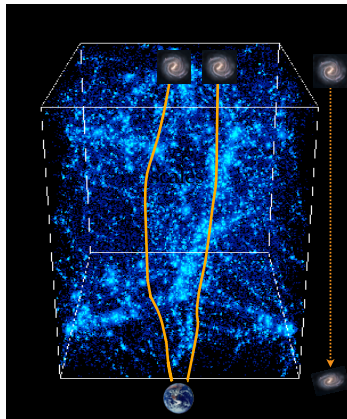


(Hildebrandt et al. 2017)

Cosmic shear, or weak cosmological lensing

Light of distant galaxies is deflected while travelling through inhomogeneous Universe. Information about mass distribution is imprinted on observed galaxy images.

- Continuous deflection: sensitive to projected 2D mass distribution.
- Differential deflection: magnification, distortions of images.
- Small distortions, few percent change of images: need statistical measurement.
- Coherent distortions: measure correlations, scales few Mpc to few 100 Mpc.



Reminder: Convergence and shear

The lens equation is the mapping from lens to source 2D coordinates. The linearized lens equation

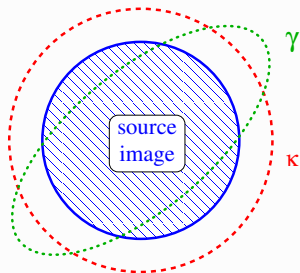
$$\frac{\partial \beta_i}{\partial \theta_j} \equiv A_{ij} = \delta_{ij} - \partial_i \partial_j \psi,$$

is described by the symmetrical 2×2 Jacobi matrix,

$$A = \begin{pmatrix} 1 - \kappa - \gamma_1 & -\gamma_2 \\ -\gamma_2 & 1 - \kappa + \gamma_1 \end{pmatrix},$$

Which defines convergence κ and shear γ .

- **convergence** κ : isotropic magnification
- **shear** γ : anisotropic stretching



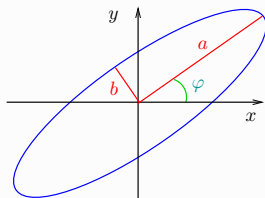
Reminder: Complex ellipticity/shear

Define complex shear

$$\gamma = \gamma_1 + i\gamma_2 = |\gamma|e^{2i\varphi};$$

The relation between convergence, shear, and the axis ratio of elliptical isophotes is then

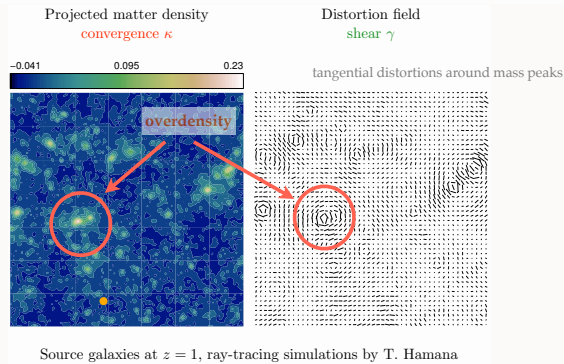
$$|\gamma| = |1 - \kappa| \frac{1 - b/a}{1 + b/a}$$



E- and B-modes: recap from part I

Shear patterns

We have seen tangential pattern in the shear field due to mass over-densities. Under-dense regions cause a similar pattern, but with opposite sign for γ . That results in radial pattern.

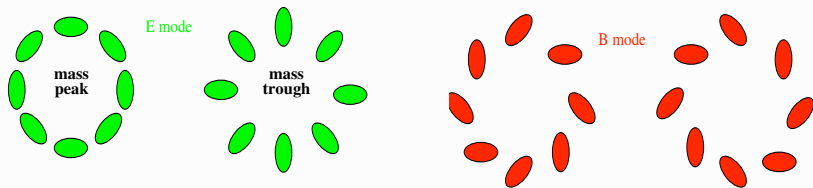


E- and B-modes: recap from part I

Shear patterns

We have seen tangential pattern in the shear field due to mass over-densities. Under-dense regions cause a similar pattern, but with opposite sign for γ . That results in radial pattern.

Under idealistic conditions, these are the only possible patterns for a shear field, the *E*-mode. A so-called *B*-mode is not generated.



E- and B-modes: recap I

Origins of a B-mode

Measuring a non-zero B-mode in observations is usually seen as indicator of residual systematics in the data processing (e.g. PSF correction, astrometry).

Other origins of a B-mode are small, of %-level:

- Higher-order terms beyond Born approximation (propagation along perturbed light ray, non-linear lens-lens coupling), and other (e.g. some ellipticity estimators)
- Lens galaxy selection biases (size, magnitude biases), and galaxy clustering
- Intrinsic alignment (although magnitude not well-known!)
- Varying seeing and other observational effects
- Non-standard cosmologies (non-isotropic, TeVeS, ...)

E- and B-modes: recap II

Measuring E- and B-modes

Separating data into E- and B-mode is not trivial.

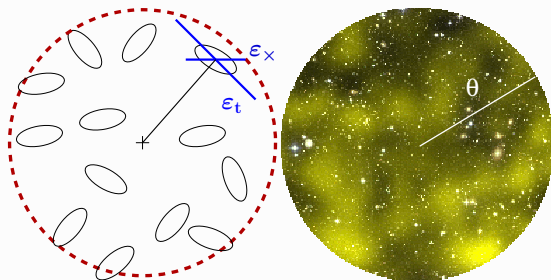
To directly obtain E and B from γ , there is leakage between modes due to the finite observed field (border and mask artefacts).

One can quantify the shear pattern, e.g. with respect to reference centre points, but the tangential shear γ_t is not defined at the center.

Solution: **filter** the shear map. (= convolve with a filter function Q). This also has the advantage that the spin-2 quantity shear is transformed into a scalar.

This is equivalent to filtering κ with a function U that is related to Q .

E- and B-modes: recap III



The resulting quantity is called **aperture mass** $M_{\text{ap}}(\theta)$, which is a function of the filter size, or smoothing scale, θ . It is only sensitive to the E-mode.

If one uses the cross-component shear γ_{\times} instead, the filtered quantity, M_{\times} captures the B-mode contribution only.

End of recap from part I.

Convergence as potential field

Again convergence κ and shear γ :

$$\frac{\partial\beta_i}{\partial\theta_j} \equiv A_{ij} = \delta_{ij} - \partial_i\partial_j\psi;$$

$$A = \begin{pmatrix} 1 - \kappa - \gamma_1 & -\gamma_2 \\ -\gamma_2 & 1 - \kappa + \gamma_1 \end{pmatrix}.$$

From this, write κ and γ as second derivatives of the potential.

Convergence as potential field

Again convergence κ and shear γ :

$$\frac{\partial\beta_i}{\partial\theta_j} \equiv A_{ij} = \delta_{ij} - \partial_i\partial_j\psi;$$

$$A = \begin{pmatrix} 1 - \kappa - \gamma_1 & -\gamma_2 \\ -\gamma_2 & 1 - \kappa + \gamma_1 \end{pmatrix}.$$

From this, write κ and γ as second derivatives of the potential.

$$\kappa = \frac{1}{2} (\partial_1\partial_1 + \partial_2\partial_2) \psi = \frac{1}{2} \nabla^2 \psi; \quad \gamma_1 = \frac{1}{2} (\partial_1\partial_1 - \partial_2\partial_2) \psi; \quad \gamma_2 = \partial_1\partial_2\psi.$$

Convergence as potential field

Again convergence κ and shear γ :

$$\frac{\partial\beta_i}{\partial\theta_j} \equiv A_{ij} = \delta_{ij} - \partial_i\partial_j\psi;$$

$$A = \begin{pmatrix} 1 - \kappa - \gamma_1 & -\gamma_2 \\ -\gamma_2 & 1 - \kappa + \gamma_1 \end{pmatrix}.$$

From this, write κ and γ as second derivatives of the potential.

$$\kappa = \frac{1}{2} (\partial_1\partial_1 + \partial_2\partial_2) \psi = \frac{1}{2} \nabla^2 \psi; \quad \gamma_1 = \frac{1}{2} (\partial_1\partial_1 - \partial_2\partial_2) \psi; \quad \gamma_2 = \partial_1\partial_2\psi.$$

We can generalise the real convergence and potential, and add an imaginary field representing the B-mode. The real part is the E-mode,

$$\psi = \psi^E + i\psi^B; \quad \kappa = \kappa^E + i\kappa^B,$$

which are related by the Poisson equations,

$$\nabla^2 \psi^{E,B} = 2\kappa^{E,B}.$$

Note that ψ^B and κ^B do not correspond to physical mass over-densities.

E- and B-mode potential, convergence, and shear I

The shear can be computed as

$$\gamma_1 + i\gamma_2 = \frac{1}{2} (\partial_1 \partial_1 \psi^E - \partial_2 \partial_2 \psi^E) - \partial_1 \partial_2 \psi^B + i \left[\partial_1 \partial_2 \psi^E + \frac{1}{2} (\partial_1 \partial_1 \psi^B - \partial_2 \partial_2 \psi^B) \right].$$

Now, we can write the E-, B-, and mixed EB-mode power spectrum.

$$\begin{aligned} \langle \hat{\kappa}^E(\ell) \hat{\kappa}^E(\ell') \rangle &= (2\pi)^2 \delta_D(\ell - \ell') P_\kappa^E(\ell), \\ \langle \hat{\kappa}^B(\ell) \hat{\kappa}^B(\ell') \rangle &= (2\pi)^2 \delta_D(\ell - \ell') P_\kappa^B(\ell), \\ \langle \hat{\kappa}^E(\ell) \hat{\kappa}^B(\ell') \rangle &= (2\pi)^2 \delta_D(\ell - \ell') P_\kappa^{EB}(\ell), \end{aligned}$$

and can derive (from $\hat{\gamma}(\ell) = e^{2i\beta} \hat{\kappa}(\ell)$, see last years' TD) for the correlators of γ in Fourier space

$$\begin{aligned} \langle \hat{\gamma}(\ell) \hat{\gamma}^*(\ell') \rangle &= (2\pi)^2 \delta_D(\ell - \ell') [P_\kappa^E(\ell) + P_\kappa^B(\ell)], \\ \langle \hat{\gamma}(\ell) \hat{\gamma}(\ell') \rangle &= (2\pi)^2 \delta_D(\ell + \ell') e^{4i\beta} [P_\kappa^E(\ell) - P_\kappa^B(\ell) + 2iP_\kappa^{EB}(\ell)]. \end{aligned}$$

Real-space correlation function (2PCF)

Fourier-transforming the last two expressions results in shear two-point correlators in real space,

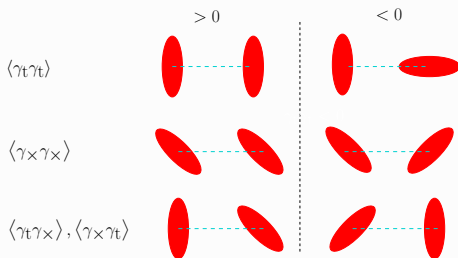
$$\begin{aligned}\langle \gamma(\boldsymbol{\theta})\gamma^*(\boldsymbol{\theta} + \boldsymbol{\vartheta}) \rangle &= \langle \gamma\gamma^* \rangle(\boldsymbol{\vartheta}) = \mathcal{F}[\langle \hat{\gamma}(\boldsymbol{\ell})\hat{\gamma}^*(\boldsymbol{\ell}') \rangle](\boldsymbol{\vartheta}); \\ \langle \gamma\gamma \rangle(\boldsymbol{\vartheta}) &= \mathcal{F}[\langle \hat{\gamma}(\boldsymbol{\ell})\hat{\gamma}(\boldsymbol{\ell}') \rangle](\boldsymbol{\vartheta});\end{aligned}$$

But these correlators are very closely related to the shear two-point correlation functions ξ_+ and ξ_- , that we defined on day 1 (part I):

$$\begin{aligned}\xi_+(\boldsymbol{\vartheta}) &= \langle \gamma_t\gamma_t \rangle(\boldsymbol{\vartheta}) + \langle \gamma_\times\gamma_\times \rangle(\boldsymbol{\vartheta}) \\ \xi_-(\boldsymbol{\vartheta}) &= \langle \gamma_t\gamma_t \rangle(\boldsymbol{\vartheta}) - \langle \gamma_\times\gamma_\times \rangle(\boldsymbol{\vartheta})\end{aligned}$$

Recall: 2PCF

Correlation of the shear at two points yields four quantities



Parity conservation $\longrightarrow \langle \gamma_t \gamma_x \rangle = \langle \gamma_x \gamma_t \rangle = 0$

The two components of the shear **two-point correlation function** (2PCF) are defined as

$$\xi_+(\vartheta) = \langle \gamma_t \gamma_t \rangle(\vartheta) + \langle \gamma_x \gamma_x \rangle(\vartheta)$$

$$\xi_-(\vartheta) = \langle \gamma_t \gamma_t \rangle(\vartheta) - \langle \gamma_x \gamma_x \rangle(\vartheta)$$

Due to statistical isotropy & homogeneity, these correlators only depend on ϑ .

2PCF and E-/B-mode power spectra I

Ignoring the imaginary part, we have thus two observables (ξ_+ , ξ_-) and two unknowns (P_κ^E, P_κ^B). We can derive, using the orthogonality of the Bessel function,

$$P_\kappa^E(\ell) = \pi \int_0^\infty d\vartheta \vartheta [\xi_+(\vartheta)J_0(\ell\vartheta) + \xi_-(\vartheta)J_4(\ell\vartheta)],$$

$$P_\kappa^B(\ell) = \pi \int_0^\infty d\vartheta \vartheta [\xi_+(\vartheta)J_0(\ell\vartheta) - \xi_-(\vartheta)J_4(\ell\vartheta)].$$

So, **in principle**, the E-/ and B-mode power spectra can be computed separately, but **not in practice**, since this requires information about the shear correlation that is unobservable, towards 0 and ∞ separation.

→ We have to further filter the field for a better separation.

Aperture mass

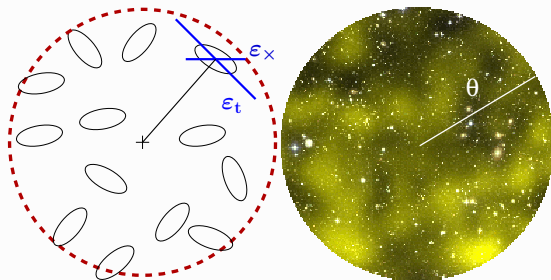
Earlier, we introduced the aperture-mass as convolution of the shear field with a filter Q ,

$$M_{\text{ap}}(\theta, \boldsymbol{\vartheta}) = \int d^2\vartheta' Q_\theta(|\boldsymbol{\vartheta} - \boldsymbol{\vartheta}'|) \gamma_t(\boldsymbol{\vartheta}')$$

and claimed that this was equivalent of convolving the convergence with another filter U ,

$$M_{\text{ap}}(\theta, \boldsymbol{\vartheta}) = \int d^2\vartheta' U_\theta(|\boldsymbol{\vartheta} - \boldsymbol{\vartheta}'|) \kappa^{\text{E}}(\boldsymbol{\vartheta}'), \quad (1)$$

(Kaiser et al. 1994, Schneider 1996).

E-/B-mode separation with M_{ap} I

It is clear that M_{ap} (M_{\times}) is sensitive to the E-mode (B-mode) of the shear field γ .

When choosing Q such that its support is finite, with $Q(\theta) = 0$ for $\theta > \theta_{\text{max}}$, the E-/B-mode separation is achieved on a finite interval.

To get this separation at the second-order level, let's take the variance of the aperture-mass: Square $M_{\text{ap}}(\theta, \vartheta)$ and average over circle centres ϑ (Schneider et al. 1998).

E-/B-mode separation with M_{ap} II

Square $M_{\text{ap}}(\theta, \vartheta)$ and average over circle centres ϑ :

$$\begin{aligned} \langle M_{\text{ap}}^2 \rangle(\theta) &= \int d^2\vartheta' U_\theta(|\vartheta - \vartheta'|) \int d^2\vartheta'' U_\theta(|\vartheta - \vartheta''|) \langle \kappa^{\text{E}}(\vartheta') \kappa^{\text{E}}(\vartheta'') \rangle \\ &= \dots = \frac{1}{2\pi} \int d\ell \ell \hat{U}^2(\theta\ell) P_\kappa^{\text{E}}(\ell). \end{aligned}$$

Analogous equations for B- and mixed modes are

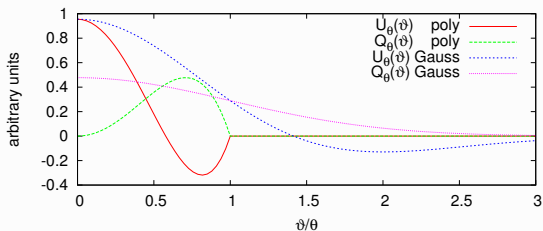
$$\begin{aligned} \langle M_\times^2 \rangle(\theta) &= \frac{1}{2\pi} \int d\ell \ell \hat{U}^2(\theta\ell) P_\kappa^{\text{B}}(\ell); \\ \langle M_{\text{ap}} M_\times \rangle(\theta) &= \frac{1}{2\pi} \int d\ell \ell \hat{U}^2(\theta\ell) P_\kappa^{\text{EB}}(\ell). \end{aligned}$$

Note: Typically, the filter function U depends on the scale ϑ normalized to the radius θ , $U_\theta(\vartheta) = U(\vartheta/\theta)$. In Fourier space this then becomes $\hat{U}(\theta\ell)$.

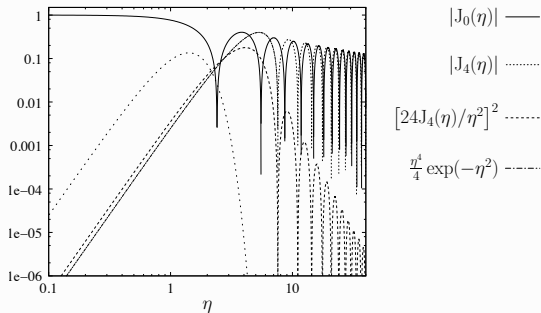
For many choices of U , \hat{U}^2 is a narrow pass-band. Thus, the aperture-mass dispersion filters out a small range of ℓ -modes around $\ell \sim \text{const } \theta^{-1}$.

E-/B-mode separation with M_{ap} III

Real space.

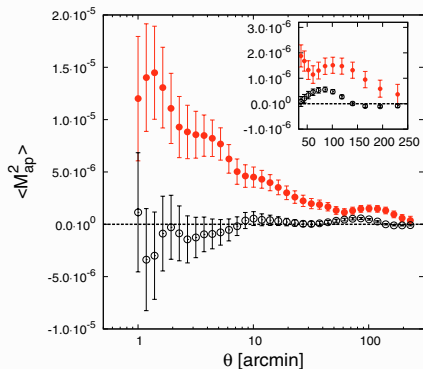


Filter functions in Fourier space.

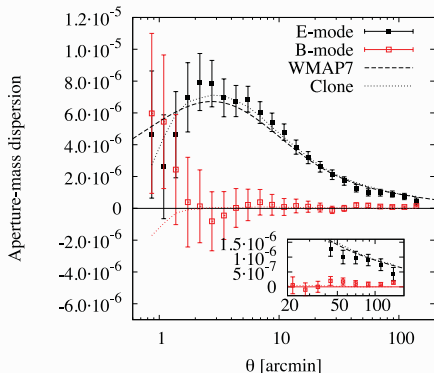


Aperture-mass dispersion measurements

CFHTLS 2007 versus CFHTLenS 2013.



From (Fu et al. 2008).



From (Kilbinger et al. 2013).

Galaxy-galaxy lensing: Overview

Correlation between high- z galaxy shapes and low- z galaxy positions.

E.g. average tangential shear around massive galaxies.

Provides mass associated with galaxy sample.

- Galaxy halo profiles from kpc to Mpc
- Mass-to-light ratio

In combination with other tracers of matter (galaxy clustering, cosmic shear, velocity correlations, X-ray emission, ...):

- Galaxy bias. Properties such as linearity, scale-dependence, stochasticity
- Test of General Relativity

Can be done quasi model-independent since two or more observables trace same matter field, but with different biases.

Tangential shear and surface mass I

In an exercise you can derive the relation between tangential shear and encompassed projected surface mass,

$$\langle \gamma_t \rangle (\theta) = \bar{\kappa}(\leq \theta) - \langle \kappa \rangle (\theta).$$

No assumption about mass distribution is made here!

We will re-write this equation defining the *surface mass excess* $\Delta\Sigma$.

Before that: brief reminder of relation between lensing convergence and matter density from last year.

Reminder: Convergence and cosmic density contrast

Back to the lensing potential

- Since $\kappa = \frac{1}{2}\Delta\psi$:

$$\kappa(\boldsymbol{\theta}, \chi) = \frac{1}{c^2} \int_0^\chi d\chi' \frac{(\chi - \chi')\chi'}{\chi} \Delta_{\boldsymbol{\theta}}\phi(\chi'\boldsymbol{\theta}, \chi')$$

- Terms $\Delta_{\chi'\chi'}\phi$ average out when integrating along line of sight, can be added to yield 3D Laplacian (error $\mathcal{O}(\phi) \sim 10^{-5}$).
- Poisson equation

$$\Delta\phi = \frac{3H_0^2\Omega_m}{2a} \delta \quad \left(\delta = \frac{\rho - \bar{\rho}}{\rho} \right)$$

$$\rightarrow \kappa(\boldsymbol{\theta}, \chi) = \frac{3}{2}\Omega_m \left(\frac{H_0}{c} \right)^2 \int_0^\chi d\chi' \frac{(\chi - \chi')\chi'}{\chi a(\chi')} \delta(\chi'\boldsymbol{\theta}, \chi').$$

Tangential shear and surface mass I

In an exercise you have derived the relation between tangential shear and encompassed projected surface mass,

$$\langle \gamma_t \rangle (\theta) = \bar{\kappa}(\leq \theta) - \langle \kappa \rangle (\theta).$$

Now we are ready to re-write equation defining the *surface mass excess* $\Delta\Sigma$.

Surface mass excess

Assume a single lens at (angular diameter) distance D_l . Approximate for this case the expression of the convergence

$$\kappa(\boldsymbol{\theta}, \chi) = \frac{3}{2} \Omega_m \left(\frac{H_0}{c} \right)^2 \int_0^\chi d\chi' \frac{(\chi - \chi')\chi'}{\chi a(\chi')} \delta(\chi' \boldsymbol{\theta}, \chi').$$

and write D_s for the distance of the source, and D_{ls} for the distance between lens and source. Write all distances as proper, not comoving distances, express the density contrast in terms of the density, $\delta = \Delta\rho/\bar{\rho}$, and use the critical density ρ_{crit} .

Tangential shear and surface mass II

Assume that the lens mass distribution ρ extends over the interval $[D_1 - \Delta D/2; D_1 + \Delta D/2]$.

$$\kappa(\boldsymbol{\theta}) = \frac{4\pi G}{c^2} \frac{D_1 D_{1s}}{D_s} \int_{D_1 - \Delta D/2}^{D_1 + \Delta D/2} dD \Delta\rho(D\boldsymbol{\theta}, D).$$

Define the *critical surface mass density*

$$\Sigma_{\text{cr}}^{-1}(\boldsymbol{\theta}) := \frac{4\pi G}{c^2} \frac{D_1 D_{1s}}{D_s}$$

to write convergence as

$$\kappa(\boldsymbol{\theta}) = \frac{\Sigma(\boldsymbol{\theta})}{\Sigma_{\text{cr}}}. \quad (2)$$

[Why is Σ_{cr} called *critical* surface mass?]

With that, we define the surface mass excess

$$\Delta\Sigma(\leq \boldsymbol{\theta}) := \langle \gamma_t \rangle(\boldsymbol{\theta}) \Sigma_{\text{cr}} = \bar{\Sigma}(\boldsymbol{\theta}) - \langle \Sigma \rangle(\boldsymbol{\theta}).$$

Statistical galaxy-galaxy lensing (GGL) I

The convergence or tangential shear defined in the last slides depend linearly on the mass distribution ρ , or Σ . So it seems to be a first-order statistic.

However, when measured statistically using a population of foreground galaxies, it can be written as two-point correlation function. The convergence is then the correlation of background lensing convergence and foreground galaxy position.

If we write the latter as galaxy over-density δ_g , we get

$$\begin{aligned}
 \langle \kappa \rangle (\theta) &= \langle \kappa(\boldsymbol{\vartheta}) \delta_g(\boldsymbol{\vartheta} + \boldsymbol{\theta}) \rangle_{\boldsymbol{\vartheta}} \\
 &= \Sigma_{\text{cr}}^{-1} \bar{\rho} \int dD \langle \delta(D\boldsymbol{\theta}, D) \delta_g(D_1\boldsymbol{\theta}, D_1) \rangle \\
 &= \Sigma_{\text{cr}}^{-1} \bar{\rho} \int dD \xi_{\delta_g}(\sqrt{(D\theta)^2 + (D - D_1)^2}).
 \end{aligned}$$

Statistical galaxy-galaxy lensing (GGL) II

Properties of statistical GGL

- Circular averages of tangential shear: robust against (some) systematic, e.g. large-scale modes of PSF residuals cancel out.
CFHTLenS: 25% fields had to be discarded for cosmic shear, none for GGL.
- Simple null tests:
 - $\langle \gamma_{\times} \rangle$ around foreground objects (parity mode, should vanish).
 - $\langle \gamma_t \rangle$ around random points, or special points that should not be correlated with foreground sample such as chip corners, field centres, stars.
- Higher SNR compared to cosmic shear:
 - correlation with tracers of dense matter regions;
 - one shape instead of two;
- Can use spectroscopic galaxies for foreground sample.

Parenthesis: galaxy bias I

Simple bias

GGL measures the cross-correlation between galaxies and dark (more precisely: total) matter, $\langle \delta_g \delta \rangle$. This correlation is non-zero since galaxies trace the underlying matter.

Simplest model: linear, constant, deterministic bias:

$$\delta_g = b\delta.$$

From that it follows that

$$\langle \delta_g \delta_g \rangle(\theta) = b^2 \langle \delta \delta \rangle(\theta); \quad \langle \delta_g \delta \rangle(\theta) = b \langle \delta \delta \rangle(\theta),$$

or in Fourier space

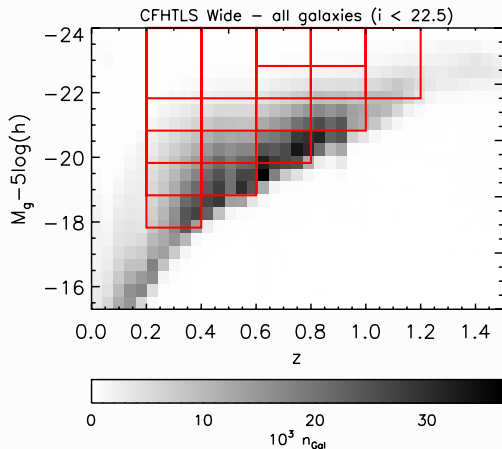
$$P_{gg}(k) = b^2 P_{mm}(k); \quad P_{gm}(k) = b P_{mm}(k).$$

Parenthesis: galaxy bias II

Properties

- The bias depends on the galaxy properties (type, color, luminosity, ...), and can be measured for different populations (e.g. early/late-type).
- Bias is redshift-dependent. Difficult to measure since degenerate with z -dependent selection effects. Volume-limited samples: Bias tends to increase with z : galaxies are more rare objects at higher z , situated in more extreme environments (halo centres).

Sample selection for galaxy bias measurement



Sample selection in absolute magnitude and redshift, from (Coupon et al. 2012).
Samples in horizontal boxes have same absolute magnitudes and are volume-limited.

Galaxy bias extended I

More complex bias models

- Scale-dependence, $b(\theta)$, or $\hat{b}(\hat{k})$. In particular on small scales, bias is not constant.
- Non-linear bias

$$\delta_g = b_1\delta + b_2\delta^2 + b_3\delta^3 + \dots$$

- Stochastic bias

Relation between δ_g is not deterministic ($\delta_g = b\delta$) but stochastic. In a statistical picture, the two fields δ_g and δ can be interpreted as realizations of random fields with joint pdf $p(\delta_g, \delta)$. The study of stochastic biasing is trying to quantify this joint pdf.

Galaxy bias extended II

At second-order level, one can measure the variances of both fields, and their cross-correlation. If the fields are correlated, one can write down the following two relations:

$$b = \frac{\sigma_g}{\sigma} = \sqrt{\frac{\langle \delta_g^2 \rangle}{\langle \delta^2 \rangle}}; \quad r = \frac{\sigma_{gm}^2}{\sigma_g \sigma} = \frac{\langle \delta_g \delta \rangle}{\sqrt{\langle \delta_g^2 \rangle \langle \delta^2 \rangle}}$$

introducing a correlation coefficient $r = -1 \dots 1$ between both fields.

In the above ratio cosmology dependence (dm correlation function or power spectrum) mainly drops out!

Allows for model-independent measurement.

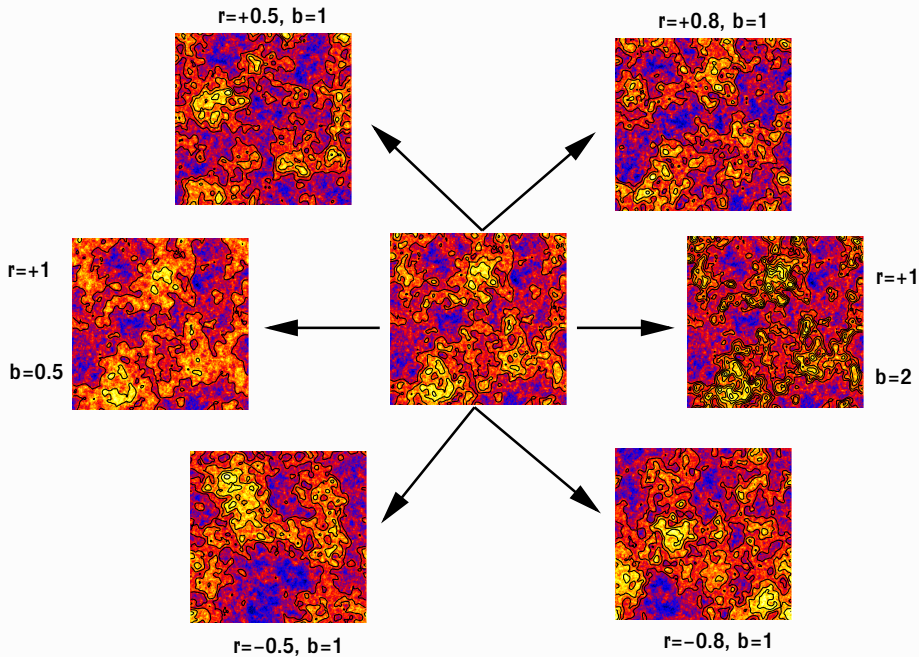


Illustration of correlated fields, from [P. Simon, PhD thesis, 2005].

GGL: model-independent measurement of b/r

Idea:

Combine weak lensing and galaxy clustering to determine b and r .

- Galaxy clustering $\langle \delta_g^2 \rangle$
- Galaxy-galaxy lensing $\langle \delta_g \delta \rangle$
- Cosmic shear $\langle \delta^2 \rangle$

Cosmic shear is the most difficult to measure, so first measurements only used GC and GGL.

Form ratio:

$$\frac{\langle \delta_g \delta \rangle(\theta)}{\langle \delta_g \delta_g \rangle(\theta)} = \frac{br}{b^2} = \frac{b}{r}.$$

Any cosmology-dependence, e.g. of clustering, drops out in the ratio. These density correlations are projected to weak-lensing observables, and b and r (if constant) can directly be measured.

GGL: Aperture measures I

How can we trace the galaxy and dark-matter over-densities with weak lensing?

Use aperture measures

$$\langle N^2 \rangle(\theta), \langle NM_{\text{ap}} \rangle(\theta), \langle M_{\text{ap}}^2 \rangle(\theta)$$

to trace

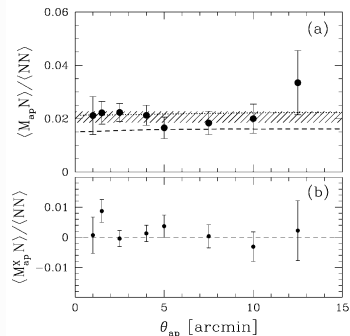
$$\langle \delta_g^2 \rangle, \langle \delta_g \delta \rangle, \langle \delta^2 \rangle.$$

Difficulty: Structure along all redshifts contribute to cosmic shear $\langle M_{\text{ap}}^2 \rangle$, not only mass associated with foreground galaxy sample δ_g .

Solutions:

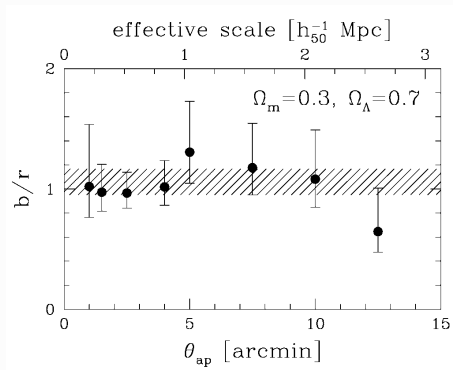
- Choose background sample such that maximum lensing efficiency coincides with foreground redshift.
- Add correction functions with minor dependency on cosmology (geometry).

GGL results: model-independent measurement of b/r

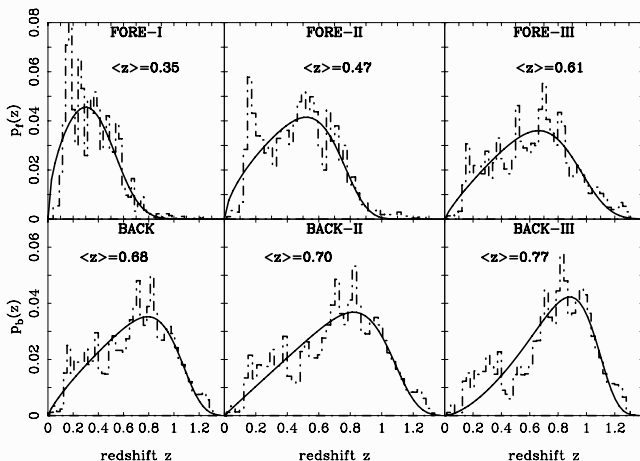


$$\mathcal{R} = \frac{r\Omega_m}{100b} [(5.8 - 1.6\Omega_m^{0.63}) + (4.6 - 2.6\Omega_m^{0.63})\Omega_\Lambda^{1.23}].$$

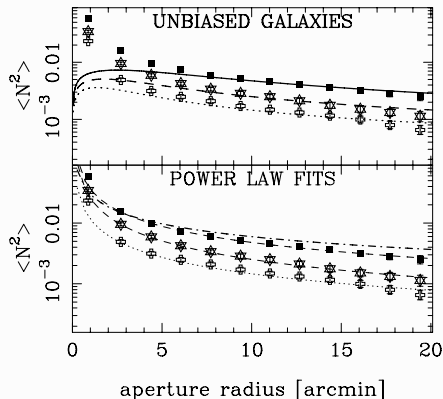
Observed ratio \mathcal{R} (a), and B-mode (b); b/r (right) from (Hoekstra et al. 2001).



Main result: no scale-dependence found (on observed scales).

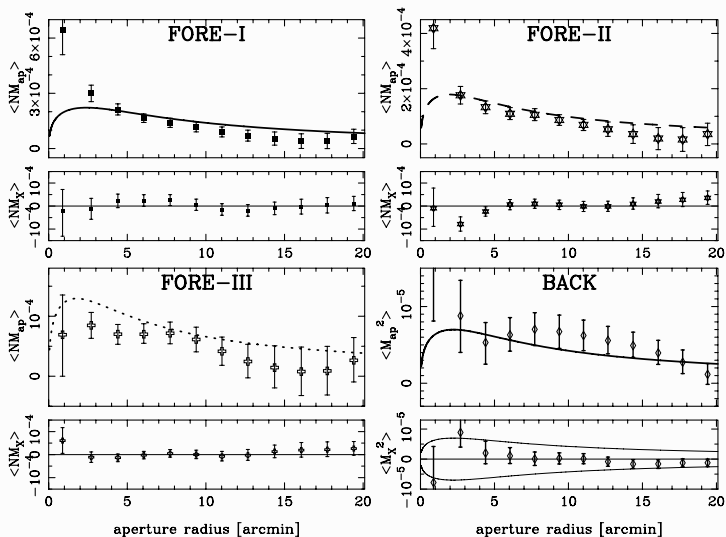
GGL results: model-indep. measurement of b and r I

Redshift distributions for GaBoDS samples, estimated from COMBO-17. From (Simon et al. 2007), GaBoDS (Garching-Bonn Deep Survey).

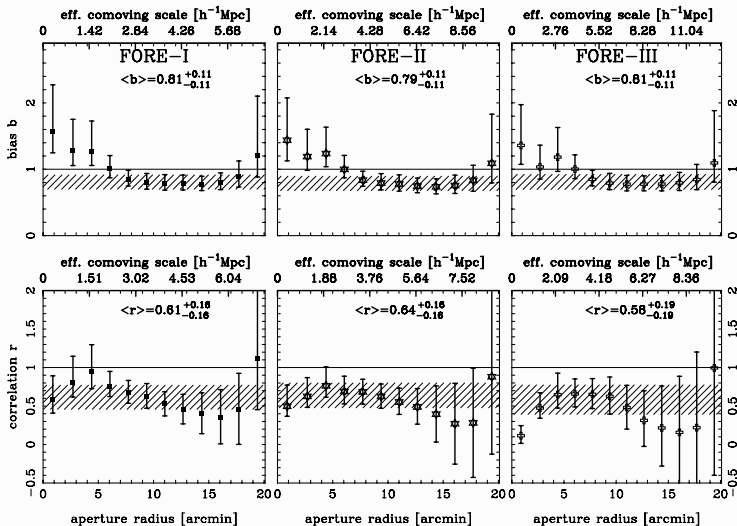
GGL results: model-indep. measurement of b and r II

Filled boxes, open stars, open crosses = FORE-I, FORE-II, FORE-III.

Galaxy clustering: Bias on small scales is not constant, but scale-dependent. Stronger galaxy clustering than from constant bias. (Simon et al. 2007), GaBoDS (Garching-Bonn Deep Survey).

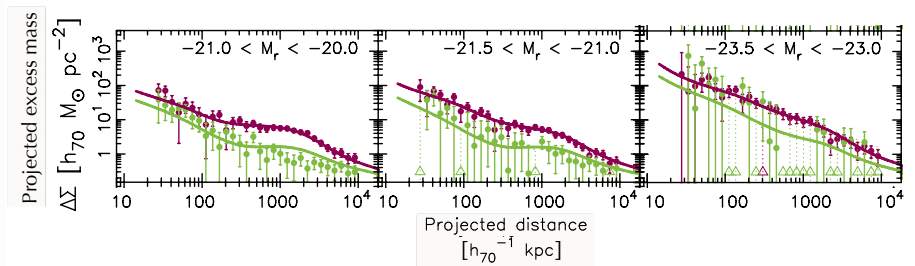
GGL results: model-indep. measurement of b and r III

GGL and cosmic shear. (Simon et al. 2007), GaBoDS (Garching-Bonn Deep Survey).

GGL results: model-indep. measurement of b and r IV

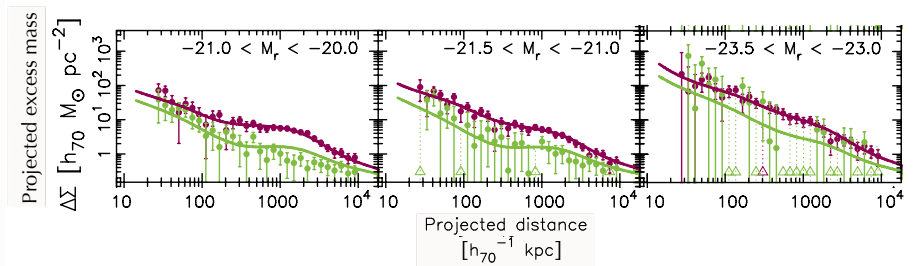
Bias and correlation coefficient. (Simon et al. 2007), GaBoDS (Garching-Bonn Deep Survey).

GGL: HOD model measurements

increasing luminosity \rightarrow 

Purple=red early-type galaxies; Green=blue late-type galaxies. From (Velandar et al. 2014).

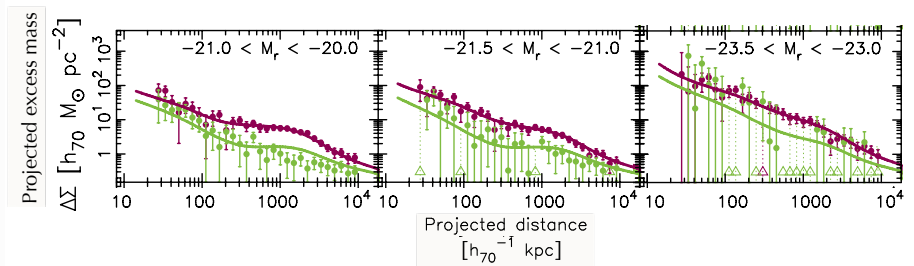
GGL: HOD model measurements

increasing luminosity \rightarrow 

Purple=red early-type galaxies; Green=blue late-type galaxies. From (Velandar et al. 2014).

- Red galaxies have larger associated mass than blue galaxies.
- Excess mass increases with luminosity. **Light traces mass.**

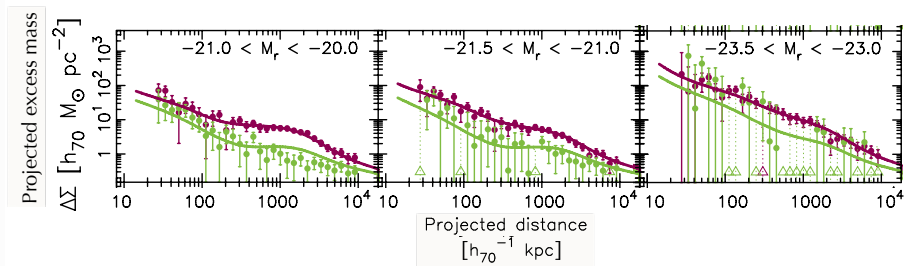
GGL: HOD model measurements

increasing luminosity \rightarrow 

Purple=red early-type galaxies; Green=blue late-type galaxies. From (Velandar et al. 2014).

- Red galaxies have larger associated mass than blue galaxies.
- Excess mass increases with luminosity. **Light traces mass.**
- Bump at 1 Mpc for low-luminosity red galaxies, disappears at higher L .
Red satellite galaxies.

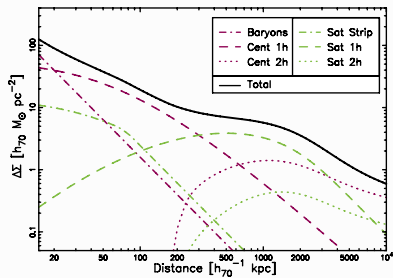
GGL: HOD model measurements

increasing luminosity \rightarrow 

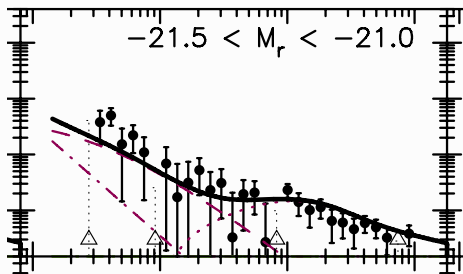
Purple=red early-type galaxies; Green=blue late-type galaxies. From (Velandar et al. 2014).

- Red galaxies have larger associated mass than blue galaxies.
- Excess mass increases with luminosity. **Light traces mass.**
- Bump at 1 Mpc for low-luminosity red galaxies, disappears at higher L .
Red satellite galaxies.
- Bump at slightly larger scale for blue galaxies. **2-halo term, from clustered nearby galaxies.**

GGL: HOD model

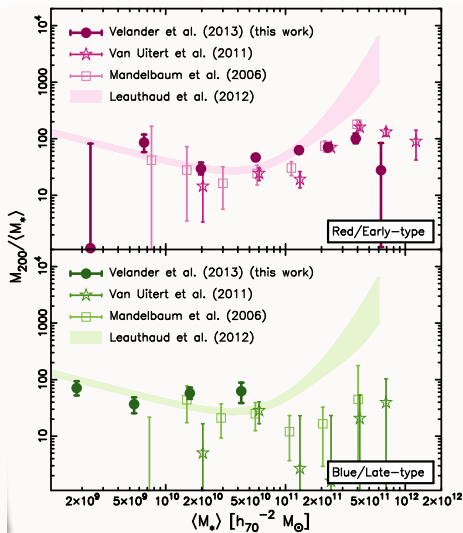
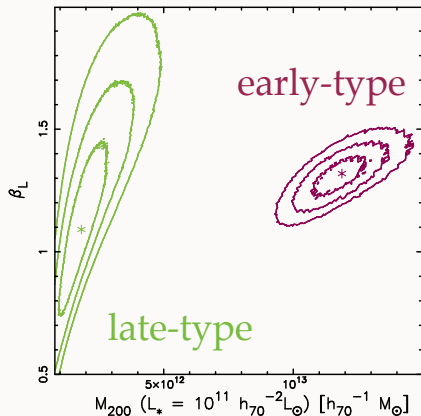


HOD model, (Vander et al. 2014).



GGL: M/L parameters

$$M_{200} = M_{0,L} \left(\frac{L}{L_{\text{fid}}} \right)^{\beta_L}$$



(Velander et al. 2014).

Shear bias

For ~~basically~~ all shape measurement methods: observed shear \neq true shear.
This is called **shear bias**.

Reminder: Write as multiplicative and additive bias:

$$\langle \varepsilon_{\alpha}^{\text{obs}} \rangle = g_{\alpha}^{\text{obs}} = (1 + m_{\alpha})g_{\alpha}^{\text{true}} + c_{\alpha}; \quad \alpha = 1, 2.$$

There is also ellipticity bias, which is different:

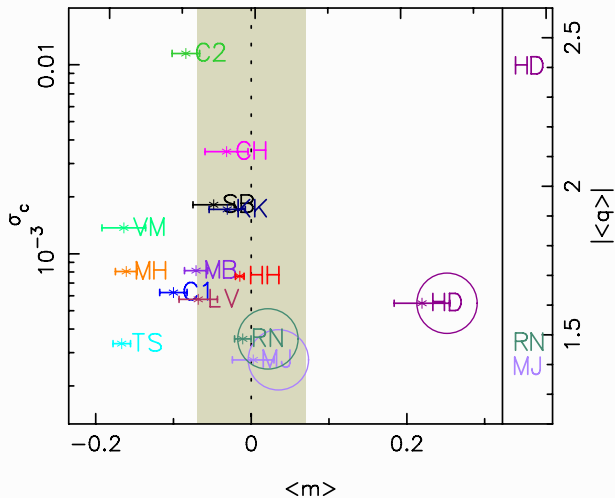
$$\varepsilon_i^{\text{obs}} = (1 + m'_i)\varepsilon_i^{\text{true}} + c'_i; \quad i = 1, 2.$$

Typical values:

year	program	Δm	Δc	$\sigma(c)$
2006	STEP I	0.1		10^{-3}
2012	CFHTLenS	0.06	0.002	
2013	great3	0.01	10^{-3}	
2014	DES	0.03–0.04	10^{-3}	
2016	KiDS	0.01–0.02	$8 \cdot 10^{-4}$	
2021	Euclid required	$2 \cdot 10^{-3}$	$5 \cdot 10^{-4}$	

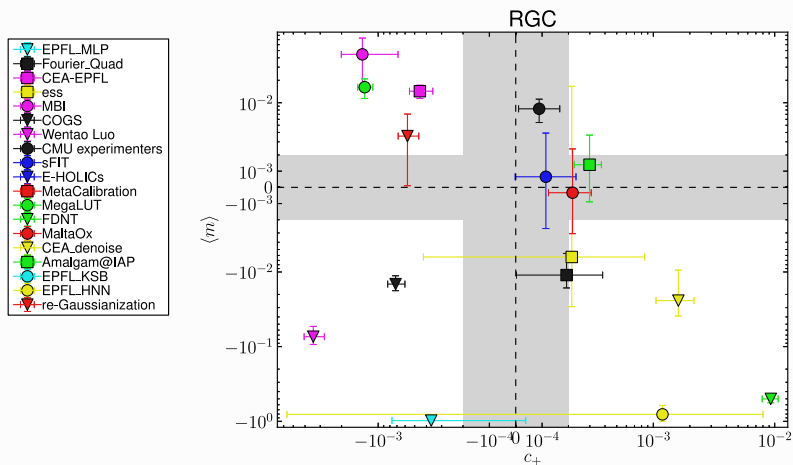
Shear bias and simulations I

From the STEP I shear measurement challenge (Heymans et al. 2006).



Shear bias and simulations II

From the great3 shear measurement challenge (Mandelbaum et al. 2015).



Shear bias and simulations III

Interprete with caution!

- Small biases because simulations are not realistic enough? E.g. constant PSF, analytical galaxy light distributions, simplistic noise, (constant shear)
- Simulation (challenges) only address part of the problem. Usually no blended galaxy images, star-galaxy separation, color effects, ...
- Calibrated or un-calibrated?

Amplitude of m, c not that important, since they can be calibrated emirically.
What counts are $\Delta m, \Delta c$ after calibration!

More on this in a few slides.

Shear bias and simulations IV

A very general statement (see Part I day 2):

Most ellipticity estimators are non-linear pixel light distribution. Noise then creates biases in the estimator. This is called **noise bias**.

Thus, observed shear needs to be de-biased (calibrated) using simulations.

There are a few unbiased estimators:

- Not normalised to total flux: maybe unbiased, but very large variance
- Bayesian estimators, sample posterior distribution, unbiased if correct model, likelihood and prior.

Prior needs to be estimated from simulations or deep survey!

Sources of bias

Reminder:

- Noise bias
- Model bias
 - Model-fitting method: incorrect model, complex galaxy morphology
 - Direct estimation: inappropriate filter function for weighted moments; truncated eigenfunction decomposition
 - Ellipticity gradients
 - Color gradients
- PSF residuals
- CTI (charge transfer inefficiency)
- Selection effects (population biases). Detection probability depends on ellipticity, orientation with PSF, pixel scale
- **New:** Environmental effects
 - Unresolved faint galaxies

Shear calibration

The bias should be *robust* for method to be *calibratable*.

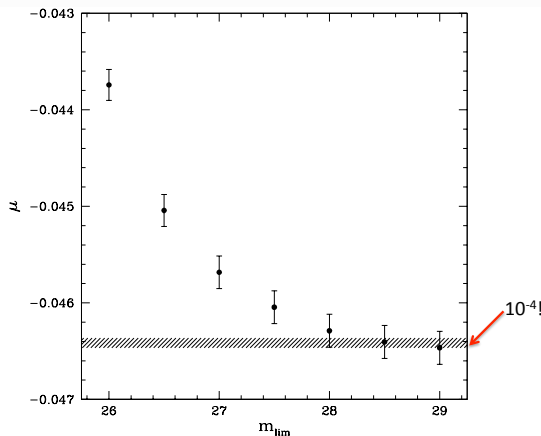
Define *sensitivity* as dependence of bias with respect to parameters, or

$$|\partial m / \partial p_i|, \quad \text{for } \mathbf{p} = \text{set of parameters.}$$

A method is calibratable, see (Hoekstra et al. 2017), if

- the sensitivity is small (otherwise simulation sampling in p too costly)
- does not depend on too many parameters
- those parameters can be measured accurately (e.g. intrinsic ellipticity dispersion σ_ε from Euclid Deep Survey \rightarrow requirement on accuracy of measured σ_ε sets area of calibration fields)
- those parameters can be reasonably simulated to estimate sensitivity
- difficult if parameter is correlated with shear signal (e.g. local galaxy density with large-scale structure, correlated with shear signal, magnification)

Shear calibration: Unresolved faint galaxies I



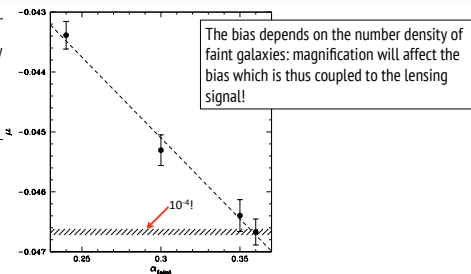
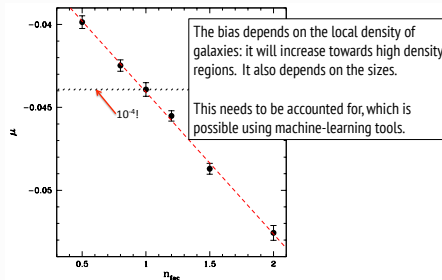
Overall values on y -axis (amplitude of m) not really important, will be corrected for.

Need simulation up to very high depth, until plateau in m is reached ($\partial m / \partial m_{\text{lim}} = 0$).

Error bars need to decrease to match hashed region.

Multiplicative bias m (here μ) for galaxies $20 < m < 24.5$ as function of limiting magnitude of simulated galaxies. From (Hoekstra et al. 2017).

Shear calibration: Unresolved faint galaxies II



Shear calibration from simulations: tricks of the trade I

Again: multiplicative and additive bias,

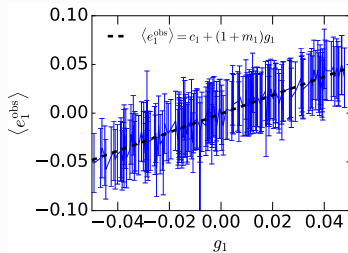
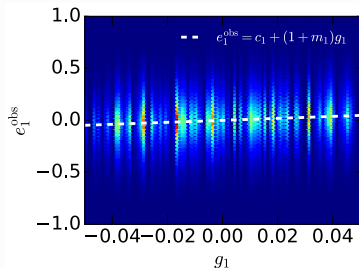
$$\langle \varepsilon_\alpha^{\text{obs}} \rangle = g_\alpha^{\text{obs}} = (1 + m_\alpha) g_\alpha^{\text{true}} + c_\alpha; \quad \alpha = 1, 2.$$

for sample of galaxies with vanishing intrinsic ellipticity $\langle \varepsilon_\alpha^{\text{I}} \rangle = 0$.

How can we determine the multiplicative bias?

Simple method

From linear fit of many simulated pairs $(\varepsilon_\alpha^{\text{obs}}, g_\alpha^{\text{true}})$.

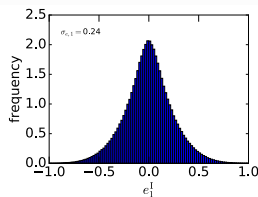


Shear calibration from simulations: tricks of the trade II

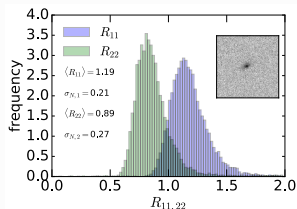
Error on best-fit m_α given by width in ε^{obs} (including measurement errors), g^{true} , and stochasticity of galaxy images (from pixel noise),

$$\sigma_{m,\alpha} = \frac{1}{\sqrt{N}} \sqrt{\sigma_{R,\alpha}^2 + \frac{\sigma_{S,\alpha}^2}{\sigma_{g,\alpha}^2}}$$

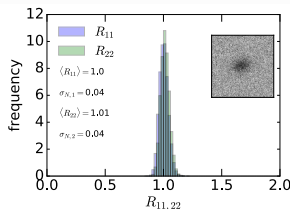
Second terms is dominant in most cases.



Ell. distribution.



Stochasticity for low SNR. Stochasticity for high SNR.



Shear calibration from simulations: tricks of the trade

III

Noise suppression

Simulate pairs of galaxies with same shear and **orthogonal** intrinsic ellipticity (rotated by 90 degrees),

$$\varepsilon_A^I + \varepsilon_B^I = 0.$$

This however does not mean that the *observed* ellipticity vanishes, due to:

- Measurement stochasticity
- Ellipticity bias, if depends on galaxy orientation wrt PSF, shear, (pixelization)
- Selection effects, one pair member might drop out of sample

Shear calibration from simulations: tricks of the trade

IV

More advanced noise suppression: ring test. Simulate n galaxies with equidistant intrinsic ellipticity on ring around 0.

Derivative method

Write shear bias for individual galaxies, and as matrix equation (Huff & Mandelbaum 2017):

$$\epsilon_{\alpha}^{\text{obs}} = \mathbf{R}g^{\text{true}} + \mathbf{c}$$

The **shear response** tensor \mathbf{R} generalizes m : $1 + m_{\alpha} = R_{\alpha\alpha}$.

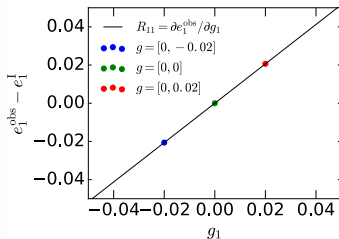
To get population bias, average over measured shear responses $\langle R \rangle$, and correct measured ellipticities by $\langle R \rangle^{-1}$.

Measure individual \mathbf{R} as numerical derivatives

$$R_{\alpha\beta} = \frac{\partial \epsilon_{\alpha}^{\text{obs}}}{\partial g_{\beta}}$$

by simulating the same galaxy several times with small added shear $\pm \Delta g_{\alpha} \sim 0.02$. With **same noise realisation** this measurement is extremely precise!

Shear calibration from simulations: tricks of the trade V



This measurement is independent of ellipticity (observed and intrinsic) and thus removes the main uncertainty of error!

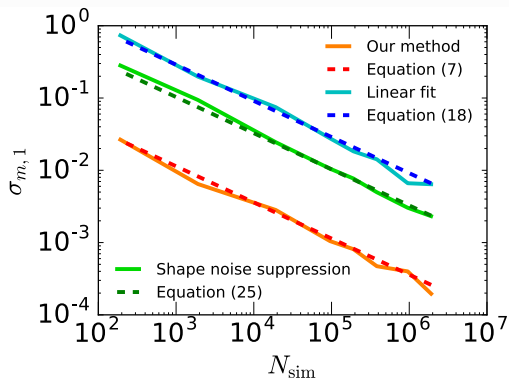
Note: For a different noise realisation, the obtained \mathbf{R} can be quite different. But the use of many simulated galaxy images assures the sampling of the distribution of R , no additional error is introduced on the population bias. Error on bias estimate:

$$\sigma_{m,\alpha} = \frac{\sigma_{R,\alpha}}{\sqrt{N}}$$

This method requires a factor of several hundred fewer image simulations.

Shear calibration from simulations: tricks of the trade

VI



From (Pujol et al. 2019).

Bibliography I

 Bartelmann M & Maturi M 2017 *Scholarpedia* **12**, 32440.

 Bartelmann M & Schneider P 2001 *Phys. Rep.* **340**(4-5), 297–472.

 Coupon J, Kilbinger M, McCracken H J, Ilbert O, Arnouts S & al. 2012 *A&A* **542**, A5.

 L, Semboloni E, Hoekstra H, Kilbinger M, van Waerbeke L & al. 2008 *A&A* **479**, 9–25.

 Heymans C, Van Waerbeke L, Bacon D, Berge J, Bernstein G & al. 2006 *MNRAS* **368**, 1323–1339.

 Hildebrandt H, Viola M, Heymans C, Joudaki S, Kuijken K & al. 2017 *MNRAS* **465**, 1454–1498.

 Hoekstra H, Viola M & Herbonnet R 2017 *MNRAS* **468**, 3295–3311.

 Hoekstra H, Yee H K C & Gladders M D 2001 *ApJ* **558**, L11–L14.

 Huff E & Mandelbaum R 2017 *arXiv* **1702.02600**.

Bibliography II

-  Kaiser N, Squires G, Fahlman G & Woods D 1994 *in* ‘Clusters of galaxies, Proceedings of the XIVth Moriond Astrophysics Meeting, Méribel, France’ p. 269.
-  Kilbinger M 2015 *Reports on Progress in Physics* **78**(8), 086901.
-  Kilbinger M, Fu L, Heymans C, Simpson F, Benjamin J & al. 2013 *MNRAS* **430**, 2200–2220.
-  Mandelbaum R 2018 *ARA&A* **56**, 393–433.
-  Mandelbaum R, Rowe B, Armstrong R, Bard D, Bertin E & al. 2015 *MNRAS* **450**, 2963–3007.
-  Pujol A, Kilbinger M, Sureau F & Bobin J 2019 *A&A* **621**, A21.
-  Schneider P 1996 *MNRAS* **283**, 837.
-  Schneider P, Kochanek C S & Wambsganss J 2006 *Gravitational Lensing: Strong, Weak and Micro* Springer Berlin Heidelberg.
-  Schneider P, Van Waerbeke L, Jain B & Kruse G 1998 *MNRAS* **296**, 873–892.

Bibliography III

-  Simon P, Hetterscheidt M, Schirmer M, Erben T, Schneider P & al. 2007 *A&A* **461**, 861–879.
-  Vander M, van Uitert E, Hoekstra H, Coupon J, Erben T & al. 2014 *MNRAS* **437**, 2111–2136.